Interfacial Binding Sites for Cholesterol on TRP Ion Channels

Anthony G. Lee[1,*]
[1]School of Biological Sciences, University of Southampton, Southampton, United Kingdom

ABSTRACT   Transient receptor potential (TRP) channels are members of a large family of ion channels located in membranes rich in cholesterol, some of whose functions are affected by the cholesterol content of the membrane. Here, cholesterol binding to TRPs is studied using a docking procedure that allows the transmembrane surface of a TRP to be swept rapidly for potential binding sites at the interfaces on the two sides of the membrane. Cholesterol docking poses determined in this way match 89% of the cholesterol hemisuccinate molecules in published TRP structures when cholesterol hemisuccinate molecules unlikely to represent typical bound cholesterols are excluded. TRPs are tetrameric, with large clefts at the interfaces between subunits; cholesterol poses are located in hollows, largely within these clefts. Comparison of cholesterol poses with phospholipid binding sites suggests that binding of cholesterol to a TRP need not result in displacement of phospholipid molecules from the TRP surface.

SIGNIFICANCE   Transient receptor potential (TRP) channels are located in membranes rich in cholesterol, and the cholesterol content of the membrane can affect TRP function. This article reports a study of cholesterol binding to 81 TRPs. The binding sites for cholesterol detected here correspond to hollows on the transmembrane surfaces of the TRPs, located between protein ridges. It is shown that cholesterol molecules can adopt a variety of poses within these hollows so that binding is unlike binding at a typical ligand binding site where a single binding pose predominates. Comparison between resolved phospholipid molecules and the cholesterol binding poses suggests that phospholipids and cholesterol will often bind at different sites on the TRP surface.

INTRODUCTION

Members of the transient receptor potential (TRP) superfamily of cation channels play important roles in a wide variety of multicellular organisms in both excitable and nonexcitable cells (1). The superfamily contains seven subfamilies, TRPA (ankyrin), TRPC (canonical), TRPM (melastatin), TRPML (mucolipin), TRPN (*Drosophila* NOMPC), TRPP (polycystin), and TRPV (vanilloid); an eighth subfamily, TRPY, is found only in yeast. The TRPs are all tetramers of identical or homologous subunits, each subunit containing six transmembrane (TM) helices in a domain-swapped arrangement, S1–S4 forming the voltage-sensor-like domain (VSLD) with S5 and S6 forming the pore domain. This arrangement results in a particularly rough TM surface ([Fig. 1](#)) with a deep cleft between neighboring subunits, with the left-and right-hand edges of the cleft

being formed by the VSLD domains and the back of the cleft being formed by two of the pore domains. Although an intracellular (IC) location has been suggested for some TRPs (2), most are located in the outer membranes of cells, membranes that, in animals, have a high content of cholesterol (3). The functions of many TRPs are sensitive to the cholesterol content of the membrane, including TRPM3, TRPM7, TRPM8, TRPV1, and TRPV3 (4–6). Further, TRPM3 is activated, and TRPC5 is inhibited by pregnenolone sulfate (7,8), a steroid that binds to the $GABA_A$ receptor (9) at sites in which docking studies show that cholesterol also binds (unpublished data). The observed effects of cholesterol on TRP function could follow from changes in the mechanical properties of the membrane or be due to direct binding of cholesterol to the channel protein (10).

An important question that first needs to be addressed is whether a cholesterol molecule colliding with the TM surface of a membrane protein sees a totally undifferentiated surface or whether it sees particular sites ("hot spots") where it would prefer to reside. Crystallographic structures
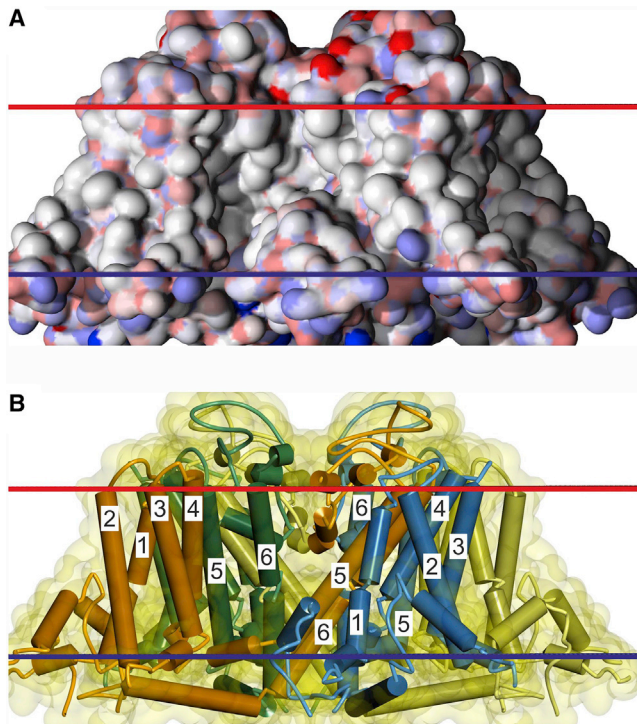
FIGURE 1 (*A*) shows the TM surface of TRPM4 (PDB: 6BQR) with the deep cleft between subunits A (*left*) and B (*right*). (*B*) shows the TM helices for subunits A (*orange*), B (*blue*), C (*green*), and D (*yellow*). TM helices in subunits A and B are numbered, together with TM helices 5 and 6 of subunit C. Red and blue bars show the locations of the membrane surfaces as calculated by OPM for the EC and IC sides, respectively. To see this figure in color, go online.

of some G-protein-coupled receptors (GPCRs) show small numbers of resolved cholesterol molecules on the protein surface, suggesting that binding sites for cholesterol do exist, although there is a possibility that some of the resolved cholesterols are crystallization artifacts (reviewed in (11)). Of course, it is also possible that there are binding sites for cholesterol not identified in structural studies, either because molecules bound at these sites are too mobile to be resolved or because the overall resolution is too low. Although no crystallographic or cryogenic electron microscopy (cryo-EM) structures of TRPs show bound cholesterol, some do show bound cholesterol hemisuccinate (CHS) molecules (Table 1), with CHS, a water-soluble derivative of cholesterol (Fig. 2 *A*), being used to stabilize many membrane proteins; CHS is used instead of cholesterol because of its solubility in maltoside detergents (12). The fact that CHS molecules used during protein purification are retained despite later detergent removal steps (13) suggests that the CHS could be bound at sites of relatively high affinity. CHS and cholesterol have similar effects on the physical properties of lipid bilayers and on membrane protein function (14), but the relationship between cholesterol and CHS binding needs to be defined. Methods additional to crystallography and cryo-EM will

therefore be needed to define the pattern of cholesterol binding to TRPs.

Although the majority of cholesterol molecules in a lipid bilayer are anchored by their –OH groups at the interface between the hydrophobic core of the bilayer and the polar lipid headgroup region (3), a small proportion are thought to locate with their –OH groups deep within the bilayer (15–17). The –OH groups of these deep cholesterol molecules, lying within the central core of the bilayer where disorder is highest, have been shown using molecular dynamics (MD) and docking approaches to hydrogen bond to suitable acceptors and donors on membrane proteins, including GPCRs and TRP channels (17,18). Here, a docking approach using AutoDock Vina (19) is used to study how cholesterol molecules, anchored at the membrane interfaces, bind to TRP channels at sites referred to as interfacial sites to distinguish them from the deep cholesterol binding sites studied previously.

To help define binding sites for cholesterol, a number of binding motifs such as the CRAC, CARC, and CCM motifs have been proposed, but these have proved to be of limited value (20–22); a recent MD study identifying hydrophobic pockets that bind cholesterol on Kir2.2 channels found that none contained cholesterol-binding motifs (23). Part of the problem is that although hydrogen bonding to the cholesterol –OH plays an important part in binding, much of the hydrogen bonding at interfacial sites is not to protein residues but to the headgroup and backbone regions of neighboring phospholipids or to water; of the resolved CHSs bound to TRP channels (Table 1), only 40% show hydrogen bonding to the protein.

Binding of cholesterol and phospholipids to membrane proteins has been studied extensively using MD methods (24–27). These studies have provided much important information about lipid binding, particularly about the dynamics of the process, but the studies require very long simulation times to ensure convergence and it is not easy to define specific binding sites from such studies (23,28). Identification of binding sites for cholesterol by MD methods is more difficult than for conventional ligands (or drugs) because of the very high concentrations of cholesterol that need to be modeled. A typical ligand binding site has an affinity in the μM range and, for example, for a solution of 1 μM ligand in water, only approximately 1 in 5×10^7 collisions with a protein surface will be ligand collisions, most of the rest being water collisions. In contrast, in a typical plasma membrane, the fraction of the lipid molecules that are cholesterol is approximately 0.3 (3) so that approximately one in three of the lipid collisions with the TM surface of a membrane protein will be cholesterol collisions. In an MD simulation, it is then necessary to distinguish between the many cholesterol molecules that are on the TM surface at any given time simply as a result of random collisions with the surface and those that can be considered to be "bound" at specific sites on the surface; MD simulations

TABLE 1   Matching of Crystallographic and Docking Results for Cholesterol Binding to TRP Channels

PDB	Side	Matched[a,b]	Unmatched[b,c]
TRPC4 Ion Channel			
5Z96	IC	A801, B801, C801, D801	
6GLK	IC	A1001, B1001, C1001, D1001	
TRPC5 Ion Channel			
6AEI	IC	A803, B802, C802, D802	
TRPM2 Ion Channel[d]			
6CO7	EC	A3000, B3000, C3000, D3000	
TRPM4 Ion Channel			
6BQR	EC	A1302, B1302, C1302, D1302	
	IC	A1301, B1301, C1301, D1301	
	IC	A1303, B1303, C1303, D1303	
6BQV	EC	A1302, B1302, C1302, D1302	
	IC	A1301, B1301, C1301, D1301	
	IC	A1303, B1303, C1303	D1303
6BWI	EC	A1204, B1204, C1202, D1202	[A1205], [B1203], [B1205], [C1201]
	EC		[C1203], [D1201], [D1203], [D1204]
	IC	A1207, B1206, C1204, D1205	A1206[e], A1209[e], B1208[e], D1206[e]
	IC	A1208, B1207, C1205, D1207	
TRPM7 Ion Channel			
5ZX5	EC	A1303, A1304, C1301, D1302	
	IC	A1301, A1302, A1305, B1301	
	IC	B1302, C1302, D1301, D1303	
TRPML3 Ion Channel			
5W3S	EC	A601, B602, C606, D605	A606, B601, C607, D602
	IC	A605, B604, C602, D604	

[a]Rmsd between crystallographic CHS molecule and docked cholesterol less than 6.5 Å.

[b]Crystallographic CHS named as in PDB file.

[c]Entries in brackets may not be good models for cholesterol binding based on the separation between the cholesterol O atom of CHS and the interface, as described in the text and shown in Fig. S1.

[d]Crystallographic steroid modeled as cholesterol.

[e]CHS highly tilted (56°–65°) and matched by cholesterol docking poses rejected on the basis of tilt angle (>30°).

for GPCRs and ion channels suggest that cholesterol molecules collide with most of the TM surface of the protein with just a few sites where cholesterol has a higher probability of binding (23–25,28). An additional problem in identifying cholesterol binding sites follows from the fact that in a membrane, the high concentration of cholesterol means that the affinity of a site for cholesterol needs not be high to ensure a high degree of occupancy of the site. The high affinity and specificity of a typical ligand binding site is due to multiple structurally specific interactions between the ligand and the protein residues making up the site (29). In contrast, cholesterol binding sites need not be deep energy wells into which a cholesterol molecule falls to occupy a single well-defined conformational state but can be shallow energy wells able to accommodate a cholesterol molecule in a range of binding poses, as shown in MD simulations of GPCRs (25,28) and Kir2.2 channels (23). This is consistent with crystallographic studies of GPCRs in which binding poses for cholesterol molecules at a given site on a given protein differ between its various reported

structures (11). Mobility of cholesterol molecules in a binding site makes it more difficult to define the protein residues contributing to the site, a problem made even more difficult by the fact that neighboring residues will be in contact with cholesterol molecules as a result of random collisions of cholesterol with the surface.

Here, a molecular docking approach is used to sweep the TM surface of TRP channels for potential binding sites for cholesterol, a method used previously to study binding of cholesterol to GPCRs (11). Docking studies make use of protein structures generated from x-ray and cryo-EM studies and generally allow no movement of protein residues; in this regard, the conditions of a docking study are comparable to those of an x-ray or cryo-EM study in which low temperatures are used to reduce motion. A potential problem with the docking approach is then that it fails to allow for changes in structure at a binding site that might follow from ligand binding (30). However, no differences were observed between docking cholesterol to GPCR structures that contained cholesterol but from which the cholesterol
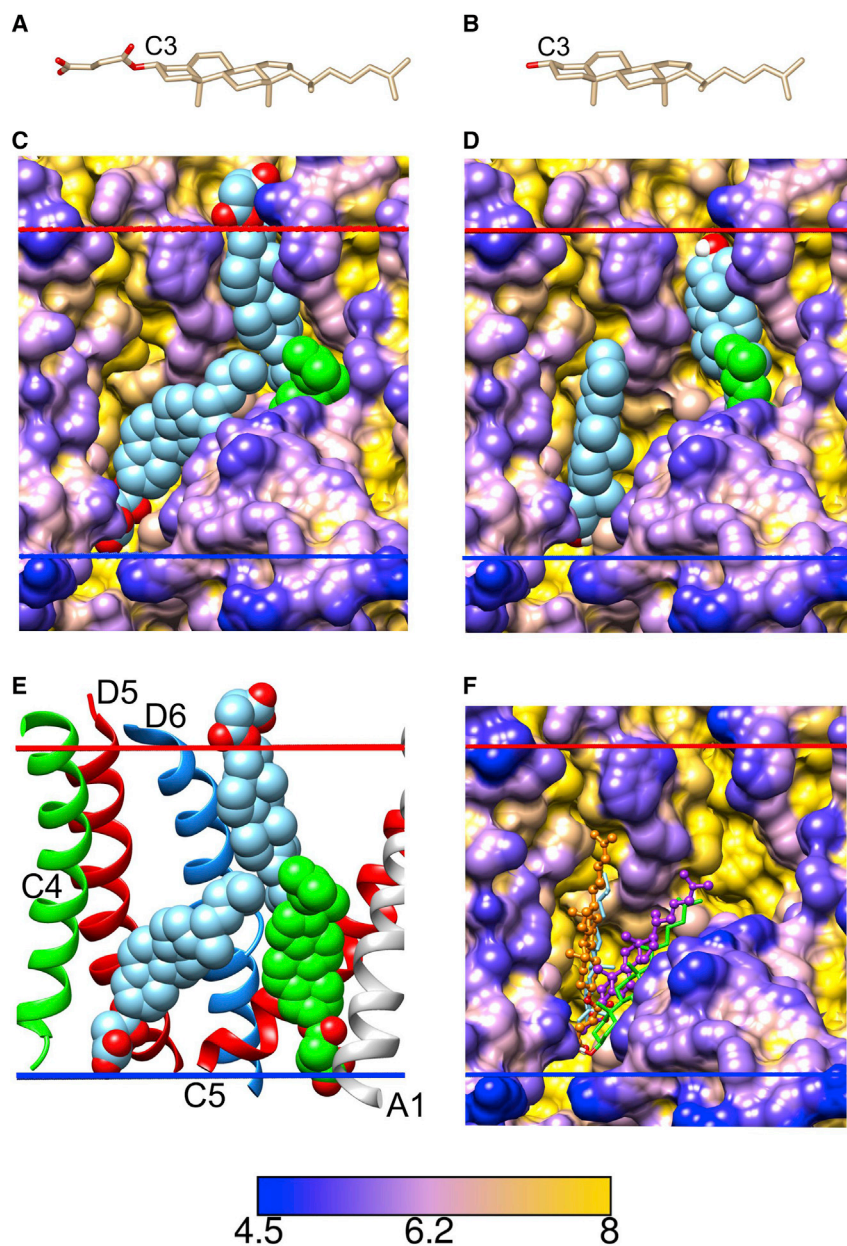
FIGURE 2 Docking and crystallographic results for the TRPM4 channel (PDB: 6BQR). (A) and (B) show, respectively, the structures of CHS and cholesterol with the C3 position marked at which either a hemisuccinate (A) or an –OH group (B) is attached. (C), (D), and (F) show protein surfaces, colored by surface depth in Å, as given by the scale at the bottom. (E) shows TM helices labeled by subunit and TM helix number. (C) and (E) show the three resolved CHS molecules per subunit, two of which (spheres, blue; oxygen, red) are clear in this view, with the third (spheres, green) being largely hidden in (C). (D) shows the selected docking poses for cholesterol, colored as in (C). (F) shows docking poses in the left-hand IC site for cholesterol and CHS. For cholesterol, the most stable docking pose (lines, blue) is shown, as in (D), together with a rejected pose (lines, green) occupying the right-hand fork of the binding site. For CHS, the most stable binding pose is shown (ball and stick, magenta) together with the second most stable binding pose (ball and stick, orange) occupying the left-hand fork of the binding site. To see this figure in color, go online.

molecules had been extracted before docking, and docking to structures that had been determined in the absence of cholesterol (11). It was concluded that ligand-induced conformation changes were absent at cholesterol binding sites on TM surfaces, a consequence of shallow energy wells that allow a cholesterol molecule to adopt a variety of binding poses within the site; binding sites for cholesterol on membrane proteins have been referred to as simple "greasy hollows" (11). A second potential problem with the docking approach is that it works with bare protein surfaces and so cannot include an explicit lipid bilayer surrounding the protein; in this, the docking approach is again comparable to the conditions found in x-ray and many cryo-EM studies. In the studies reported here, the lack of a lipid bilayer around the TM surface of a protein was ameliorated in two ways. First, competition between cholesterol and lipid fatty acyl chains for binding to the hydrophobic TM region of the protein was accounted for by reducing to zero the hydrophobic component of the total docking energy (18). Second, model interfaces were created on the extracellular (EC) and IC sides to which a cholesterol –OH group could hydrogen bond, to mimic the interactions with hydrogen-bond donors and acceptors present in the interface regions of a lipid bilayer (11).

The protocol employed generates a maximum of 200 cholesterol binding poses that must be processed to produce

a meaningful set of strong binding sites, separating such sites from weaker, background sites and from "false" sites. This cannot be done solely on the basis of the docking energies calculated by AutoDock Vina because these energies are based on a statistical scoring function and so are less reliable than calculations based, for example, on force field methods (19). Rather, the method of selection adopted was an evidence-based approach, designed to select potential binding sites whose characteristics match those of known interfacial cholesterol binding sites. An analysis of the 131 interfacial cholesterols resolved in GPCR structures showed that the maximum tilt angle between the long axis of the cholesterol ring system and the bilayer normal was 30° and that the minimum number of residues contacted by a bound cholesterol was eight (11). The criteria adopted for selecting a binding pose were therefore a tilt angle of 30° or less and a minimum number of residue contacts of eight. Because many TRP structures show C4 symmetry, an additional filtering step was applied in the TRP studies based on this symmetry (see below).

In studies of GPCRs (11), it was shown that interfacial cholesterols bind with their –OH groups close to the membrane interfaces around the protein, as given by the Orientations of Proteins in Membranes (OPM) database (31). However, binding of CHS is more complex than binding of cholesterol because CHS can anchor at an interface either through the ester group attached to C3 of the cholesterol ring or through the carboxyl group of the succinate moiety (Fig. 2, A and B). This is illustrated in Fig. 2 for TRPM4 in which three CHSs are resolved per subunit (13). On the EC side, CHS anchors at the interface via its ester group with the rest of the succinate group being above the interface (Fig. 2, C and E) so that the mode of binding closely resembles that of cholesterol (Fig. 2 D); in both cases, the membrane anchor lies close to the long axis of the cholesterol ring system. However, on the IC side, both CHS molecules bind via their succinate carboxyl groups. One of the CHSs (Fig. 2 E, green) binds with a linear structure, but the other (Fig. 2 E, blue) is bent at the ester linkage at C3 so that although the succinate group is aligned close to the bilayer normal, the rest of the CHS molecule is highly tilted. Such a bend is of course not possible for cholesterol, meaning that CHS and cholesterol might not bind to the same sites or might not bind in the same way to any given site; the relationship between the observed binding sites for CHS and any binding sites for the biologically relevant cholesterol molecule therefore needs to be established.

An important test of the success of a docking study is provided by its ability to reproduce known binding sites. Published TRP structures include a total of 88 CHSs. Of these, 81% were matched in the docking studies with cholesterol reported here (Table 1). Removing eight resolved CHS molecules judged to be less likely to represent a cholesterol binding site (see below) increases the match rate to 89%, equaling that in docking studies with GPCRs (11).

Details of all the docking results are available in Supporting Materials and Methods and on the Deep Cholesterol web site (https://deepcholesterol.soton.ac.uk).

METHODS

The docking method has been described in detail elsewhere (11). Crystal structures were identified on the OPM (http://opm.phar.umich.edu) and Protein Data Bank (PDB; https://www.rcsb.org) databases. Analysis was limited to structures with a resolution of 4 Å or better; for many cryo-EM structures, the resolution in the TM region is better than that reported for the overall structure. Structures containing gaps in TM helices within the bilayer core that could result in artifactual docking poses are noted in Table S1. Protein structure files were downloaded from the OPM database (31) and the dummy atoms marking the EC and IC interfaces converted into NH_3 groups to allow hydrogen bonding of a cholesterol molecule at the interface. Proteins were prepared for docking using the Dock Prep and AddH routines in Chimera (32), with H atoms added to the protein and to the cholesterol oxygen. Any lipids or other ligands were deleted, and for convenience, large extramembranous domains were also removed. Docking was performed using AutoDock Vina (19) running under Chimera using binding parameters appropriate for a hydrophobic environment (18). Docking was performed separately for the EC and IC monolayers, and because of the large size of the TRP tetramers, two overlapping search boxes were employed for each monolayer. The exhaustiveness value was set at 200 (11). Docking poses were sorted into clusters using simple threshold clustering (33) based on a root mean-square deviation (rmsd) between poses of less than 4 Å. Poses were filtered on the basis of cholesterol tilt angle and numbers of residue contacts using in-house Python code (see below). Five sequential Vina runs were performed to ensure complete coverage of the TM surface, the selected poses from the first run being combined with the structure file used in the first run to create the structure file to be used in the second run and so on. In a final filtering step for TRP structures showing C4 symmetry, only docking poses that appeared at equivalent positions on at least three of the four subunits were selected except for any poses in the central channel pore, as described below. In what follows, a selected docking pose will usually be referred to simply as a pose.

Results were analyzed using in-house Python code. Clustering of selected cholesterol poses for different reported structures of the same protein was performed using the DBSCAN method (33) with a threshold rmsd value of 3.5 Å and a minimum number of neighbors of two. Residues within 4 Å of a docked cholesterol were determined using the routines in Chimera. Residue depths below a theoretical bulk solvent layer around the protein were determined using the Depth server (34) with a solvent neighborhood radius of 3 Å and a minimum number of neighborhood solvent molecules of five.

RESULTS AND DISCUSSION

The protocol for identifying interfacial cholesterol binding sites

The success of the docking protocol adopted here depends on being able to define a set of criteria by which to sort through the docking poses returned by AutoDock Vina, selecting just those that corresponded to strong binding sites of the type reported in structural studies. For GPCRs, these criteria were based on an analysis of bound cholesterols in GPCR crystal structures, which showed that the average tilt angle between the long axis of the cholesterol ring

system and the normal to the two bilayer surfaces was 14.4 ± 6.7°, with a maximum tilt angle of 30°, and the average number of residues contacted by a bound cholesterol was 10.1 ± 1.5, with a range of values between 8 and 13 (11). The requirements for selection of a docking pose on a GPCR were therefore set at a maximum tilt angle for a bound cholesterol of 30° and a minimum number of contacts of eight. An analysis of resolved CHS molecules bound to TRPs (Table 1) showed that the corresponding average tilt angle was 27.1 ± 15.0°, with a maximum tilt angle of 65°, and the average number of residue contacts for a CHS was 11.5 ± 3.4, with a range of values between 2 and 16. The wider range of values for CHS than for cholesterol is likely to follow from the effect of the succinate moiety, as shown in Fig. 2 and discussed above. To minimize the number of false-positives, a conservative approach to selection was adopted and the same selection criteria were used as in the GPCR studies, that is, a maximum tilt angle for a bound cholesterol of 30° and a minimum number of contacts of 8.

The protocol for sweeping the TM region of a channel for binding sites employs separate docking runs for the EC and IC sides, with two overlapping search boxes for each side. Protein structure files were prepared in the pdbqt format required by Vina. A first docking run for one side of the membrane using one of the two search boxes for that side generally resulted in 20 poses, the maximum number returned by Vina. These poses were sorted into clusters based on an rmsd of 4 Å, and a pose was rejected if the cholesterol molecule did not meet the chosen selection criteria. For those poses assigned to clusters, the most energetically favorable pose in the cluster was chosen to represent that cluster. The poses selected from this first run were then combined with the protein structure file used in the first run to generate the pdbqt file to be used in the second run. Poses generated in the second run were then combined with the structure file used in the second run to generate the pdbqt file for the third run and so on. A total of five runs were performed, with most poses being generated in the first two runs, a few in the next two, and none in the final, fifth run. The process was repeated for the second search box for that side, and the poses from the two search boxes were combined, eliminating one copy of any pose duplicated in the region of overlap between the two boxes.

For TRP structures showing C4 symmetry, binding sites would be expected at equivalent positions on all four subunits, as was observed experimentally for CHS binding in which all bound CHS molecules fell into sets of four (Table 1); this C4 symmetry in binding provides a further criterion that can be used in the selection of docking poses. Of the 22 sets of bound CHS, 4 were not matched by any poses (Table 1), as discussed below. Of the remaining 18 sets, 17 had matching poses for all 4 CHSs in a set, but 1, for PDB: 5ZX5 on the EC side, had matching poses for only 3 CHSs in the set, the unmatched CHS being matched

by a cholesterol pose rejected on the basis of a high tilt angle. In light of these results, it was decided to retain docking poses that appeared at equivalent positions on at least three of the subunits for a protein showing C4 symmetry but to reject any appearing at equivalent positions on less than three subunits; this maintained a balance between rejecting false binding poses but at the same time retaining as many as possible of the "true" binding poses. Filtering on the basis of C4 symmetry was not applied to any poses in the central pore of the channel where C4 symmetry would not necessarily be expected. The effect of symmetry filtering can be illustrated by the docking results for the eight available structures for TRPM4, three of which included CHS and five of which did not (Table S1). Without symmetry filtering, docking studies for these 8 structures resulted in a total of 245 selected poses. Of these, 91% appeared in sets of four and were therefore included after symmetry selection. 5% of the selected poses appeared in sets of three and were also included after symmetry selection; 4% appeared either in sets of two or as single docking poses and were rejected. These are the final selected docking poses that are listed in Table S1 and discussed in what follows.

A comparison between docking and structural results

Docking studies are commonly judged on their ability to match any true ligand binding sites, as established by previous structural studies, with few false-positives. Here, a docking pose and a bound CHS molecule are taken as matching if their rmsd value, calculated excluding the hemisuccinate group, was less than 6.5 Å, the relatively large value taking account of the shift between the ring systems of CHS and cholesterol caused by the presence of the succinate moiety (see Fig. 2). Of the 88 resolved CHSs in published TRP structures, 71 are matched by docking poses (Table 1), which is a success rate of 81%. However, this includes a number of resolved CHSs occupying binding sites thought less likely to represent binding sites for cholesterol because of the location of the CHSs relative to the bilayer interfaces. For resolved cholesterols bound to GPCRs with their O atoms above the interface (ie, protruding into the lipid headgroup region), the average distance between the O and the interface was 2.8 ± 2.5 Å; for those below the interface (ie, located in the hydrophobic core of the bilayer), the corresponding distance was 1.12 ± 0.9 Å. For resolved CHS, the distance between the cholesterol O and the interface was 2.4 ± 1.9 Å for those above the interface, similar to that for cholesterol, but for those below the interface, the average value was 4.9 ± 2.9 Å, much larger than the value for cholesterol suggesting that the succinate moiety can anchor a CHS away from the interface. This is illustrated in Fig. S1 for the two sets of CHSs on the EC side of the PDB: 6BWI structure for TRPM4 (Table 1). As shown, the hydrophobic portions of the CHS molecules

are not located in hollows of the kind typically occupied by cholesterol and CHS (see Fig. 2) and their succinate moieties are located far above the interface predicted by OPM, too far from the protein surface to be involved in charge or hydrogen-bond interactions with the protein. A bound CHS with a cholesterol O to interface distance of more than approximately 3 Å may not, therefore, be a reliable model for a cholesterol binding site. If the eight CHS molecules falling into this category (Table 1) are excluded from the calculation of matches, the matching success rate increases to 89%.

A comparison between resolved CHS molecules and cholesterol docking poses for the PDB: 6BQR structure of TRPM4 (13) is presented in Fig. 2, showing the three CHSs resolved per subunit, all binding in the deep cleft between the VSLDs of neighboring subunits. On the EC side, the CHS bound between S6 of subunit D and S5 of subunit C (Fig. 2 E) is matched well by a cholesterol pose (Fig. 2, C and D). On the IC side, the binding site between S4 and S5 of subunit C and S5 and S6 of subunit D is bifurcated, with a CHS occupying the right-hand fork (Fig. 2, C and E). The corresponding cholesterol pose occupies the left-hand fork (Fig. 2 D), although a rejected pose occupies the right-hand branch (Fig. 2 F), this pose having been rejected on the basis of the small number (six) of residue con-

tacts. However, in a docking study with CHS, although the most energetically favorable CHS pose (docking energy -20.7 kcal mol^{-1}) occupied the right-hand branch, the second most favorable pose occupied the left-hand branch despite having essentially the same docking energy (-20.1 kcal mol^{-1}) (Fig. 2 F), illustrating small differences in the binding preferences of cholesterol and CHS.

A cluster analysis of cholesterol poses for the eight available TRPM4 structures is shown in Fig. 3 and includes four human and four mouse structures. The observation of docking poses on CHS-free mouse TRPM4 structures corresponding to the CHS binding sites on human TRPM4s suggests that large conformational changes do not occur on binding CHS so that structures without bound CHS or cholesterol can be used to determine binding sites for cholesterol, as was shown for GPCRs (11). Fig. 3 also shows that clusters are observed at sites other than those to which CHS binds and that many of the clusters contain less than the eight poses expected if cholesterol bound equally to all eight TRPM4 structures. Some of this variation in pose number per cluster could arise from sequence differences between human and mouse protein or from effects of ligand binding on protein conformation but could also follow from differences in the positions of the interface planes about the protein, as shown for GPCRs (11). Hydrogen bonding
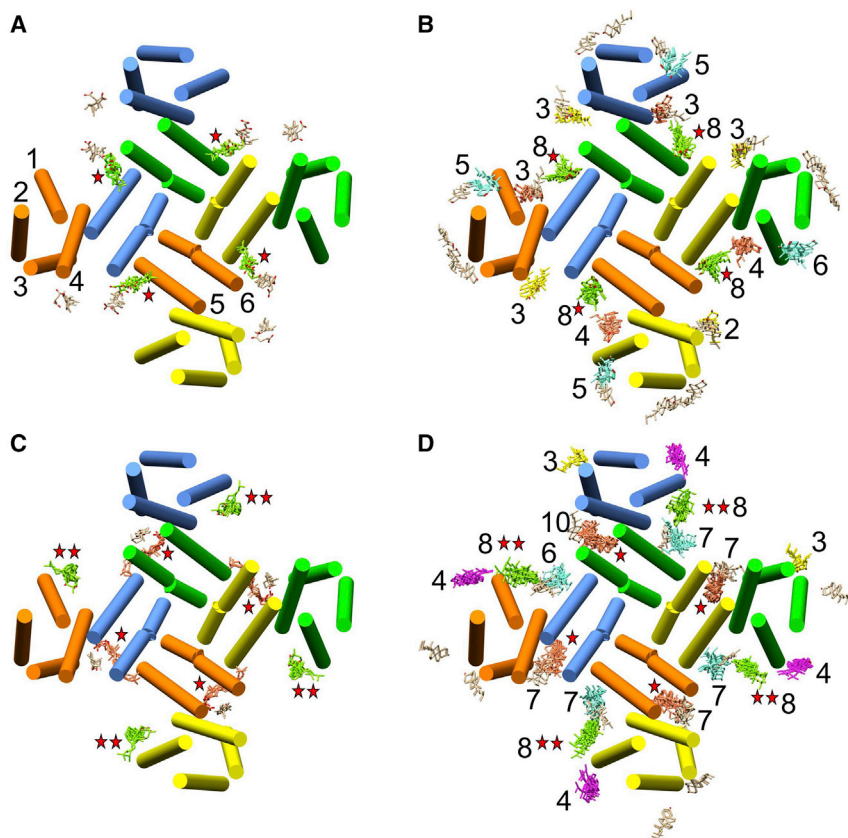

FIGURE 3 Cluster analysis of docking poses for TRPM4, with all views being from the EC side. The eight structures included in the analysis are listed in Table S1, and all structures have been aligned to PDB: 6BQR. (A) and (C) show structurally resolved CHS molecules, and (B) and (D) show cholesterol docking poses for the EC (A and B) and IC (C and D) monolayers. TM helices are colored by subunit: A, green; B, blue; C, yellow; D, orange. TM helix numbers are given for subunit D in (A). (A) and (C) show clusters of resolved CHS molecules colored by cluster, with CHS molecules not in a cluster colored tan; clusters are marked by one (IC side) or one and two (EC side) red stars. (B) and (D) show docking clusters colored by cluster and indicated by stars as in (A) and (C), with single dockings colored tan; the number of poses in each cluster is given. To see this figure in color, go online.

between a cholesterol –OH group and the interface makes a major contribution to the calculated docking energy and depends on the distance between the –OH group and the interface. The locations of the interfaces, as predicted by OPM (31), are sensitive to the distribution of charged residues in the interhelical loops close to the EC and IC interfaces, which can differ between structures (Fig. 4 C). For example, predicted interface planes for mouse PDB: 6BCO (35) are 2 Å above those for human PDB: 6BQR (Fig. 4, A and C) because of differences in loop positions on the IC side and to differences in the lengths of three regions on the IC side where the protein is unresolved (Fig. 4 C). The consequences of these differences are shown in Fig. 4 for one particular docking site on each subunit, that between S2 and S3 on the IC side (see Fig. 3 D). Although a docking pose is observed at this site for 6BCO, it is not for 6BQR

even though the positions of residues close to the docked cholesterol in 6BCO are matched well by those in 6BQR when 6BQR is aligned to 6BCO (Fig. 4 A). However, shifting the interface around 6BQR by 2 Å along the z axis so that it becomes identical to that for 6BCO results in a docking pose on 6BQR that matches that on 6BCO (Fig. 4 B). The possible significance of these differences is discussed below. It is worth noting that effects of poorly defined flexible loops and missing charged residues on the predicted locations of the bilayer interfaces around a membrane protein will apply not only to OPM but also to MD simulations.

Binding of cholesterol to TRP channels

In the TRPM4 subfamily, the three resolved CHS molecules per subunit and the corresponding cholesterol poses (Table 1) are located in narrow hollows between protein ridges located in the deep clefts between VSLDs and pore domains (Figs. 1 and S2 A). On the EC side, the hollow is between S6 of one monomer and the short pore helix of the neighboring monomer (Fig. 2), and it has been suggested that binding here could stabilize the conformation of the pore (13). On the IC side, one of the occupied hollows (Fig. 2, *right-hand side*) is located between S1 and the two short helices that precede S1, forming an inverted V shape inserted into the membrane and referred to as the pre-TM1 elbow (13). The other occupied hollow (Fig. 2, *left-hand side*) is between S4 and S5 of one subunit and S5 and S6 of the neighboring subunit. Other cholesterol poses also occupy surface hollows, mostly within the deep clefts between VSLDs (Fig. S2 A). Within many of the hollows, cholesterols adopt a range of poses, contrasting with the single binding pose commonly observed in the deep energy well typical of most ligand or drug binding sites. The most favorable pose adopted within a hollow will depend on the pattern of hydrogen bonding between the cholesterol –OH and the interface, and as described above, the position of the interface around the protein differs between structures and will fluctuate because of thermal motion of both the protein and the surrounding lipid bilayer. The range of binding poses within a hollow (Fig. S2 A) could therefore represent the variation in poses because of thermal motion in a biological membrane, as suggested previously for GPCRs (11,25,28) and Kir2.2 channels (23).

Docking results for other TRPM structures also show most poses within the deep central clefts (Table S1). The PDB: 6CO7 structure for TRPM2 from sea anemone in the closed state includes a single resolved cholesterol per subunit on the EC side (Fig. S2 B; Table 1), although it is possible that this is actually CHS because CHS was used in the purification procedure (36). No bound sterols were reported on the IC side, and the site between S4 and S5 of one subunit and S5 and S6 of the neighboring subunit, occupied by CHS in TRPM4, was occupied by the two fatty acyl chains of a phosphatidic acid (PA); a cholesterol docking
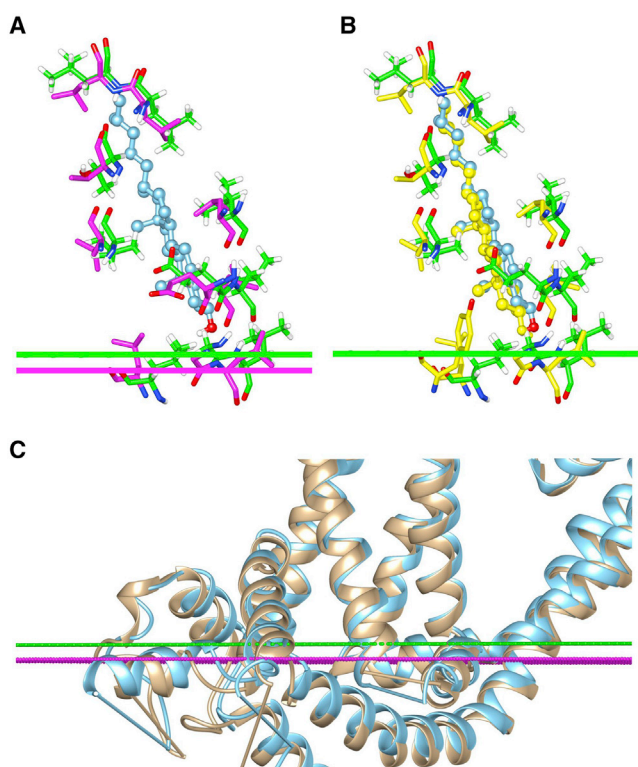

FIGURE 4 Effect of interfacial layer position on docking to mouse and human TRPM4. (*A*) and (*B*) show cholesterol docking on the IC side at the site between S2 and S3 for PDB: 6BCO (mouse) and PDB: 6BQR (human), with 6BQR aligned to 6BCO. (*A*) shows the interface planes for 6BCO (*bar*, *green*) and for aligned 6BQR (*bar*, *magenta*). The cholesterol pose at this site for 6BCO is shown in ball and stick (*blue*): there is no corresponding pose for 6BQR. Residues neighboring the cholesterol docked to 6BCO are shown in green, with the corresponding residues in the aligned 6BQR in magenta. In (*B*), the IC interface for 6BQR has been shifted by 2 Å along the z axis to be identical to that for 6BCO (*bar*, *green*). A cholesterol pose is now seen at the site for 6BQR (*ball and stick, yellow*), similar to that for 6BCO (*blue*), as in (*A*). Residues close to the docked cholesterols in 6BCO and 6BQR are shown in green and yellow, respectively. (*C*) compares protein structures (*ribbons*) on the IC side for subunit A for 6BCO (*tan*) and for aligned 6BQR (*blue*) with regions of unresolved structure shown as rods. To see this figure in color, go online.

pose overlaps one of the fatty acyl chains of the PA (Fig. S2 B; Table S1). Competition between phospholipids and cholesterol for binding on TRPs is described in more detail below. The structure of zebra fish TRPM2 in the closed state (PDB: 6DRK) (37) is markedly different from that of the closed state of sea anemone TRPM2, with the central, ion-conducting pore being connected to the middle of the hydrophobic core of the lipid bilayer by four openings between the S5/S6 pore domains of adjacent subunits (Fig. S3 A). Similar connections have been observed in two-pore K$^+$ channels and ATP-gated P2X3 channels where they are referred to as fenestrations (38); cholesterol has been shown to dock into these fenestrations (18). Two cholesterol molecules dock in the central pore of the closed zebra fish TRPM2 (Fig. S4), with their -OH groups close to a Thr or Ile residue from each subunit on the EC and IC sides, respectively (Fig. S4). Although cholesterol binding in the channel would presumably help to seal the pore against ion movement in the closed state, the fenestrations are too small to allow access of a cholesterol from the lipid bilayer into the pore, unless thermal motion results in expansion of the fenestrations. The low aqueous solubility of cholesterol would probably limit binding of cholesterol in the pore if access was only possible from the aqueous phase. Fenestrations in the closed form of human TRPM2 (PDB: 6MIX) (39) are very much smaller than those for the zebra fish protein, and only a single cholesterol molecule docks in the central pore on the EC side (Table S1). Cholesterol docking to the open form of zebra fish TRPM2 differs from that of the closed form (Fig. S3 B); on the IC side, there are no docking poses, and there is only a single docking pose in the central pore on the EC side (Table S1). In two of the structures for the closed form of TRPM8 of the collared flycatcher (PDB: 6NR2, 6NR3) (40), four cholesterol molecules are observed docked in the large entrance portal on the EC side that leads to the central pore (Fig. S5; Table S1). In a third structure (PDB: 6NR4) (40), there are two cholesterol poses in the central pore on the IC side but none on the EC side (Table S1). Cholesterol poses are also seen in the central pores of TRPV1, TRPV2, TRPV5, and TRPC6 (Table S1).

In the TRPML subfamily, TRPML3 (PDB: 5W3S) (41) shows, in the cleft between subunits, two closely spaced CHS molecules on the EC side and one on the IC side (Fig. S6; Table 1). A single cholesterol pose on the EC side is located between the two CHS sites, closest to that on the right (Fig. S6); the selected pose, the most favorable energetically, was chosen from a set of poses covering a range of positions that include the sites of the two bound CHSs. On the IC side, the single bound CHS is matched by a cholesterol pose, and there is also a pose corresponding to the site occupied by a lipid fatty acyl chain in the published structure (Fig. S6).

Docking results for the TRPV subfamily are generally similar to those for the other TRPs (Table S1). It has been suggested that a highly conserved CRAC-like sequence (K^{608}DLFRFLL^{615} in *Xenopus* TRPV4) is important in binding cholesterol in TRPV4 (42), but this is not part of the cholesterol docking sites detected here (Table S1). Similarly, it has been suggested that Arg residues in the S4-S5 loop or in S5 could be important in cholesterol binding to TRPV1 (5,43), but this is not supported by the docking results. Mutation of L581 or F582 in S5 has been shown to block the effects of cholesterol on TRPV1 currents (5), and these two residues are parts of the docking sites for cholesterol on TRPV1 (PDB: 5IRX) in the open state (44) (Table S1). Of the seven gain-of-function mutants of TRPV3 associated with Olmsted syndrome (45), two, W521 and Q580, are parts of the cholesterol docking sites on three of the TRPV3 structures (PDB: 6MHO, 6MHS, 6MHW) (45) (Table S1).

The sensitivity of cholesterol docking to the fine details of surface structure are emphasized by the structure of the open form of TRPV1 (PDB: 5IRX) (44) bound to the divalent toxin DhTx (Fig. S7). Two DhTx molecules bind on the EC side in an antiparallel fashion, degrading the original C4 symmetry to C2, with the C-terminal loop of the toxin penetrating deeper into the membrane than the N-terminal loop (44); cholesterol docking also shows C2 symmetry. In the two clefts into which C-terminal loops have inserted, there are, per subunit on the EC side, one resolved phosphatidylethanolamine (PE) and one cholesterol pose, and on the IC side per subunit, one resolved phosphatidylcholine (PC) and a cholesterol pose at the same site (Fig. S7 A). In contrast, in the two clefts into which N-terminal loops have inserted, there are per subunit, on the EC side, no resolved phospholipids and two cholesterol poses, and, on the IC side per subunit, one resolved PC but no cholesterol pose (Fig S7 B). Structures of TRPV2 (PDB: 6BWJ, 6BWM) (46) and TRPV3 (PDB: 6MHW, 6MHX) (45) with C2 symmetry also show C2 symmetry in cholesterol docking (Table S1).

TRPC3, TRPC6, and TRPC7 are activated by diacylglycerol (DAG) (47), and the cryo-EM structure of TRPC3 (PDB: 6CUD) (48) shows one DAG bound to each subunit in the central cleft on the EC side (Fig. 5 A). The –OH group of the DAG is located well below the predicted location of the interface but is close to two potential hydrogen partners K607 and N633. No selected cholesterol poses appear in this location, although a nonselected pose, rejected on the basis of a too-high tilt angle, is located in the cleft, with the cholesterol –OH hydrogen bonding with the interface (Fig. 5 A); competition between cholesterol and DAG for binding at this site is therefore likely to be weak.

Two TRPC4 structures (PDB: 5Z96, 6G1K) (49,50) show one resolved CHS per subunit (Fig. 5 B; Table 1) matched by a cholesterol docking pose (Fig. 5 B; Table 1). Both structures also contain one bound PA per subunit (49,50) located in the central cavity, with its headgroup buried deep in the membrane, away from the membrane interface
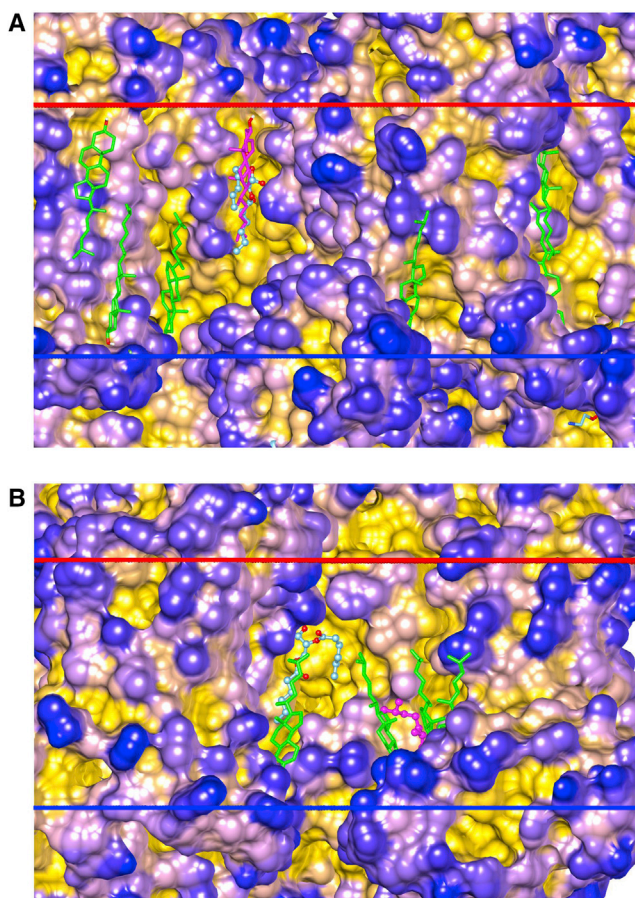
FIGURE 5 Docking of cholesterol to (*A*) TRPC3 (PDB: 6CUD) and (*B*) TRPC4 (PDB: 6GIK). Cholesterol poses are shown as lines (*green*). In (*A*), bound DAG is shown (*ball and stick*, *blue*) together with a nonselected cholesterol pose (*lines*, *magenta*) overlapping the bound DAG. (*B*) shows the bound PA (*ball and stick*, *blue*) and CHS (*ball and stick*, *magenta*). To see this figure in color, go online.

making hydrogen-bond interactions with Q569 and W573 but without any obvious positively charged partner for the negatively charged phosphate group (Fig. 5 *B*). One of the cholesterol poses on the IC side overlaps one of the PA fatty acyl chains (Fig. 5 *B*).

Competition between phospholipid and cholesterol

Docking of cholesterol to structures including resolved or partly resolved phospholipids provides clues as to how phospholipids and cholesterol might compete for binding on the surface of a TRP channel. The structure of TRPML1 (51) includes the headgroup and glycerol backbone regions of PtdIns(3,5)P$_2$ but with very little of the fatty acyl chains (Fig. 6 *A*). Whereas cholesterol poses are restricted to hollows in the central cleft, the resolved parts of PtdIns(3,5) P$_2$ are located outside the hydrophobic core of the membrane, presumably with their fatty acyl chains highly disordered on the protein ridges within the hydrophobic core,

suggesting that there will be little competition between PtdIns(3,5)P$_2$ and cholesterol for binding. Similarly, little competition is likely on TRPM8 where the headgroup and glycerol backbone regions of PtdIns(4,5)P$_2$ are located on the ridges (40) with the cholesterol poses all being in the hollows (Table S1). A lack of competition is also likely for TRPV1 (Fig. 6 *B*; (44)). Here, four PE molecules are resolved per subunit on the EC side, but a lack of large hollows extending to the EC interface means that there are no cholesterol poses on the EC side; PE can bind because PE binding is driven by polar interactions between the headgroups and regions of the protein outside the hydrophobic core of the surrounding lipid bilayer, with the flexibility of the fatty acyl chains allowing matching of the chains to the rough surface of the protein ridges. On the IC side of TRPV1, a PC binds in the hollow between S4 of one VSLD domain and S5 and S6 of the pore domain of the neighboring subunit, and as shown, there is a cholesterol pose in this region, with cholesterol competing predominantly with just one of the two fatty acyl chains (Fig. 6 *B*).

Competition between phospholipids and cholesterol for binding is particularly clear for the *Drosophila* NOMPC (TRPN) channel (Fig. 6, *C* and *D*). This structure includes eight PC molecules per subunit, four each on the EC and IC sides (52), with seven cholesterol poses per subunit, three on the EC side and four on the IC side (Table S1). Long, narrow hollows extend between the EC and IC interfaces and contain the cholesterol poses. For most of the PCs, only the upper parts of the fatty acyl chains are resolved, the chains generally being located away from the deep hollows. Where a longer length of chain is resolved, the chain adopts a more ordered, nearly all-*trans* configuration and occupies one of the hollows. In one case, an almost fully extended chain on the EC side (Fig. 6 *C*, *colored magenta*) occupies a hollow extending from the EC to the IC sides and competes with a cholesterol pose on the IC side. Of the seven cholesterol poses per subunit, only one (on the EC side) does not correspond to a site occupied by a PC fatty acyl chain, and of the eight PCs, only two show no competition with a cholesterol pose. In only one case do cholesterol poses compete with both chains of a PC. A similar pattern is observed for TRPP1 in which a single PA is observed per subunit (53) and a cholesterol pose overlaps just one of the PA chains (Table S1).

Overall, these results suggest that hot spots for binding cholesterol and phospholipid may be different so that binding of cholesterol will not necessarily result in displacement of a phospholipid, consistent with the MD simulation results of Barbera et al. (23) with the Kir2.2 channel. Further, the observation that when there is competition, a cholesterol molecule generally competes with only one of the two fatty acyl chains of the phospholipid, raises the possibility that even in these cases, binding of cholesterol may not completely displace the phospholipid, which could remain bound via just one of its two chains. This would explain
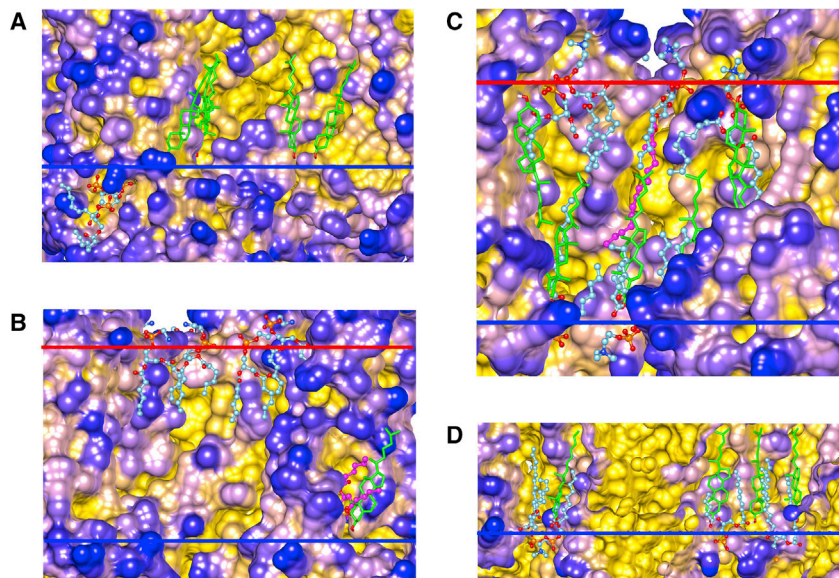
FIGURE 6 Binding of cholesterol and phospholipid to (*A*) TRPML1 (PDB: 6E7P), (*B*) TRPV1 (PDB: 5IRZ), and (*C* and *D*) TRPN (PDB: 5VKQ). Phospholipids are shown as ball and stick with (*A*) partially resolved PtdIns(3,5)P$_2$ (*blue*), (*B*) PE on the EC side (*blue*) and PC on the IC side (*magenta*), and (*C* and *D*) PC (*blue*). In (*C*), the most extended fatty acyl chain is shown in magenta. Cholesterol docking poses are shown as lines (*green*). (*D*) shows a cutaway view of the IC side to expose the bound PCs and docked cholesterols. To see this figure in color, go online.

the results of fluorescence quenching studies of cholesterol and phospholipid binding to membrane proteins, which also suggested that cholesterol is able to bind to the TM surface of a membrane protein without displacing phospholipid (54).

Assigning nonprotein density

The limited resolution of many cryo-EM structures makes it difficult to assign nonprotein densities in the TM region to particular species of lipid. Although a Y-shaped density suggests the presence of a two-chain phospholipid, a "sausage" shape could correspond to one fatty acyl chain of a phospholipid or to cholesterol or CHS; knowing whether a cholesterol docking pose is located in the region of an observed density could help with assignment. This is illustrated in Fig. 7 for three members of the TRPV subfamily. The cryo-EM structure of the closed state of TRPV2 (PDB: 5AN8), purified in the presence of CHS, showed density between TM helices S1 and S4 on the IC side just above the TRP domain, which, it was suggested could be cholesterol (55). A single cholesterol pose was observed on each subunit in just this position (Fig. 7 *A*). In a cryo-EM structure of TRPV5 in the presence of the inhibitor econazole (PDB: 6B5V), density was observed on the IC side and suggested to be due to econazole (56), but a second cryo-EM study, this time in the absence of econazole, also observed density in this region, which it was suggested could be due to cholesterol (57). Two cholesterol poses were observed on each subunit of the 6B5V structure on the IC side, one of which overlaps the suggested binding site for econazole (Fig. 7 *B*). Of the six residues assigned to the binding pocket for econazole (56), four (I428, L460, I486, I565) are local to the

docked cholesterol (Table S1). It is possible therefore that either cholesterol competes with econazole for binding at this site or the density attributed to econazole in fact is due to cholesterol.

Human TRPV6 (PDB: 6E2F) in nanodisks shows four nonprotein densities per subunit, two each on the EC and IC sides (58). The best defined of the densities on the IC side lies between S3 and S4 of one subunit and S5 and S6 of a neighboring subunit, with one end close to T479 and Q483 in the S4-S5 linker and was suggested to be either cholesterol or the acyl chain of a phospholipid (58). The density corresponds well to one of the two cholesterol poses on the IC side, with two of the residues suggested to be close to the binding site (T479 and Q483) also being local to the docked cholesterol (Fig. 7 *C*). On the EC side, a Y-shaped density between S5 and the P helix of one subunit and S1 of the neighboring subunit corresponds well to a cholesterol pose; of the seven residues suggested to be close to the binding site, five (I341, I348, Y349, P527, and L530) are local to the docked cholesterol (Fig. 7 *D*) suggesting either that cholesterol and phospholipid compete for binding at this site or that the observed density actually corresponds to a molecule of cholesterol or CHS. The second, sausage-shaped density on the EC side, close to the Y-shaped density, was located between S6 of one subunit and the P helix of the neighboring subunit (58) and could correspond to the second of the docked cholesterols on the EC side, with residues making up this site coming from S6 and the P helix of the neighboring subunit (Table S1).

CONCLUSIONS

TRPs operate in membranes rich in cholesterol, cholesterol affecting the functions of many TRPs (4,6). These effects
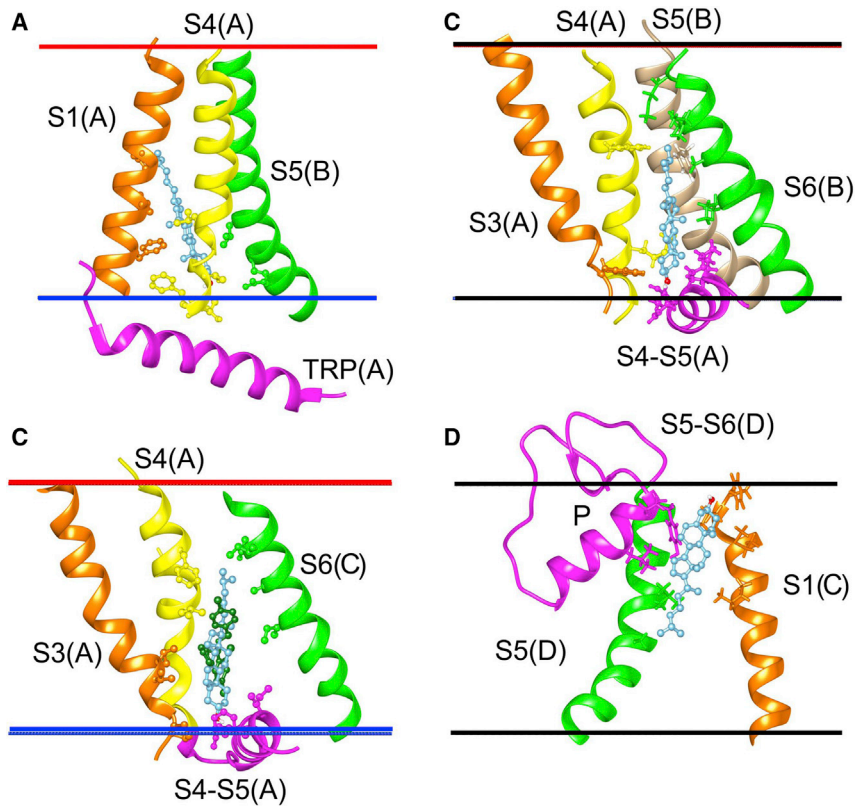
FIGURE 7 Assignment of nonprotein densities in TRPVs. In all cases, the docked cholesterol is shown as ball and stick (*blue*), and residues local to the docked cholesterol are shown as ball and stick colored by the helix to which they belong. (*A*) Docking of cholesterol to the closed state of TRPV2 (PDB: 5AN8). The docking pose is shown between S1 and S4 of subunit A and S5 of subunit B, above the TRP domain. (*B*) Docking of cholesterol to the closed state of TRPV5. The suggested binding site for econazole (*ball and stick*, *dark green*) is shown between S3 and S4 of subunit A and S6 of subunit C, above the S4-S5 linker for subunit A, with the corresponding cholesterol docking pose. (*C*) and (*D*) show docking to the EC and IC sides of TRPV6 (PDB: 6E2F), respectively. (*C*) shows S3 and S4 of subunit A and S5 and S6 of subunit B, together with the S4-S5 linker for subunit A with the corresponding docking pose. (*D*) shows S1 of subunit C and S5 of subunit D together with the S5-S6 linker and the P helix of subunit D with the corresponding docking pose. To see this figure in color, go online.

could follow either from changes in the mechanical properties of the membrane or from direct binding to the protein. Most cholesterol molecules locate in a membrane with their –OH groups close to the interfaces between the fatty acyl chain and headgroup regions of the lipids. Studies with GPCRs have shown that cholesterol –OH groups are more likely to hydrogen bond with the bilayer interfaces than with the GPCR (11). MD simulations show that cholesterol molecules interact with most of the TM surface of a GPCR or of the potassium channel Kir2.2 but with a few hot spots where cholesterol has a higher probability of binding (23,24,28). In a previous article, it was shown that a docking approach could be used to sweep the GPCR surface for cholesterol binding sites and that 89% of the resolved cholesterol molecules were matched by docking poses (11). Here, it is shown that this docking procedure can also be used to study TRPs.

TRPs adopt a tetrameric structure with deep clefts where the four VSLDs pack together (Fig. 1). As for the GPCRs, cholesterol poses were found to be located in hollows in the TM surfaces, with these hollows being located mostly in the clefts between VSLDs. Nine of the published TRP structures contain resolved CHS molecules (Table 1), with CHS commonly being used during protein purification to increase stability. Of the total of 88 resolved CHS molecules in these structures, 81% were matched by cholesterol docking poses, with this increasing to 89% if the eight CHSs

judged to be less likely to be located at a cholesterol binding site are excluded. A comparison between bound CHSs and their equivalent cholesterol docking poses suggests that cholesterol and CHS occupy similar, but not identical binding sites on TRPs in large hollows extending to the hydrophobic-polar interfaces of the membrane. Cholesterol docking studies could therefore be helpful in assigning nonprotein densities observed in cryo-EM studies; several examples are presented in Fig. 7.

Comparisons of cholesterol poses for sets of TRP structures show that cholesterol molecules adopt a variety of poses within a hollow; the hollows are not deep energy wells into which a cholesterol molecule falls to adopt a single pose, as in a typical ligand or drug binding site. The pose within a hollow that is most favorable energetically depends on the position of the interface around the TRP because of the importance of hydrogen bonding between the cholesterol −OH and the interface. The position of the interface will vary because of thermal motion of both the lipid bilayer and of the protein, and the observed variation in docking poses within a hollow could therefore represent the range of poses adopted by a cholesterol molecule because of thermal motion.

A number of cryo-EM studies of TRPs include partially resolved phospholipid molecules. Comparing these phospholipids to the cholesterol poses suggests that whereas cholesterol binding is largely restricted to long hollows

extending to the EC or IC interfaces, phospholipid binding, particularly for phosphatidylinositols, depends on interactions of the lipid headgroups with protein surfaces outside the hydrophobic core of the surrounding lipid bilayer and flexible lipid fatty acyl chains are less structurally demanding than the rigid rings of a cholesterol. It is suggested that some phospholipids and cholesterols bind at different sites on a protein surface and that when they bind at the same site, cholesterol is likely to compete with just one of the two phospholipid fatty acyl chains. Overall, these results suggest that binding of cholesterol to a TM surface will not necessarily result in the complete displacement of a phospholipid from the surface, which is in agreement with the results of earlier fluorescence quenching studies (54).

SUPPORTING MATERIAL

ACKNOWLEDGMENTS

REFERENCES

1. Venkatachalam, K., and C. Montell. 2007. TRP channels. *Annu. Rev. Biochem.* 76:387–417.

2. Agosto, M. A., I. A. Anastassov, …, T. G. Wensel. 2018. A large endoplasmic reticulum-resident pool of TRPM1 in retinal ON-bipolar cells. *eNeuro.* 5:ENEURO.0143-18.2018.

3. Song, Y., A. K. Kenworthy, and C. R. Sanders. 2014. Cholesterol as a co-solvent and a ligand for membrane proteins. *Protein Sci.* 23:1–22.

4. Levitan, I., D. Singh, and A. Rosenhouse-Dantsker. 2014. Cholesterol binding to ion channels. *Front. Physiol.* 5:65.

5. Picazo-Juárez, G., S. Romero-Suárez, …, T. Rosenbaum. 2011. Identification of a binding motif in the S5 helix that confers cholesterol sensitivity to the TRPV1 ion channel. *J. Biol. Chem.* 286:24966–24976.

6. Morales-Lázaro, S. L., and T. Rosenbaum. 2017. Multiple mechanisms of regulation of transient receptor potential ion channels by cholesterol. *In* Current Topics in Membranes. I. Levitan, ed. Academic Press, pp. 139–161.

7. Wagner, T. F., S. Loch, …, J. Oberwinkler. 2008. Transient receptor potential M3 channels are ionotropic steroid receptors in pancreatic beta cells. *Nat. Cell Biol.* 10:1421–1430.

8. Majeed, Y., M. S. Amer, …, D. J. Beech. 2011. Stereo-selective inhibition of transient receptor potential TRPC5 cation channels by neuroactive steroids. *Br. J. Pharmacol.* 162:1509–1520.

9. Laverty, D., P. Thomas, …, T. G. Smart. 2017. Crystal structures of a GABA$_A$-receptor chimera reveal new endogenous neurosteroid-binding sites. *Nat. Struct. Mol. Biol.* 24:977–985.

10. Lee, A. G. 2011. Biological membranes: the importance of molecular detail. *Trends Biochem. Sci.* 36:493–500.

11. Lee, A. G. 2019. Interfacial binding sites for cholesterol on G protein-coupled receptors. *Biophys. J.* 116:1586–1597.

12. Thompson, A. A., J. J. Liu, …, R. C. Stevens. 2011. GPCR stabilization using the bicelle-like architecture of mixed sterol-detergent micelles. *Methods.* 55:310–317.

13. Autzen, H. E., A. G. Myasnikov, …, Y. Cheng. 2018. Structure of the human TRPM4 ion channel in a lipid nanodisc. *Science.* 359:228–232.

14. Simmonds, A. C., E. K. Rooney, and A. G. Lee. 1984. Interactions of cholesterol hemisuccinate with phospholipids and (Ca^{2+}-Mg^{2+})-ATPase. *Biochemistry.* 23:1432–1441.

15. Marrink, S. J., A. H. de Vries, …, S. R. Wassall. 2008. Cholesterol shows preference for the interior of polyunsaturated lipid membranes. *J. Am. Chem. Soc.* 130:10–11.

16. Marquardt, D., F. A. Heberle, …, J. Katsaras. 2016. Lipid bilayer thickness determines cholesterol's location in model membranes. *Soft Matter.* 12:9417–9428.

17. Genheden, S., J. W. Essex, and A. G. Lee. 2017. G protein coupled receptor interactions with cholesterol deep in the membrane. *Biochim Biophys Acta Biomembr.* 1859:268–281.

18. Lee, A. G. 2018. A database of predicted binding sites for cholesterol on membrane proteins, deep in the membrane. *Biophys. J.* 115:522–532.

19. Trott, O., and A. J. Olson. 2010. AutoDock Vina: improving the speed and accuracy of docking with a new scoring function, efficient optimization, and multithreading. *J. Comput. Chem.* 31:455–461.

20. Jaipuria, G., T. Ukmar-Godec, and M. Zweckstetter. 2018. Challenges and approaches to understand cholesterol-binding impact on membrane protein function: an NMR view. *Cell. Mol. Life Sci.* 75:2137–2151.

21. Rosenhouse-Dantsker, A., D. E. Logothetis, and I. Levitan. 2011. Cholesterol sensitivity of KIR2.1 is controlled by a belt of residues around the cytosolic pore. *Biophys. J.* 100:381–389.

22. Rosenhouse-Dantsker, A. 2017. Insights into the molecular requirements for cholesterol binding to ion channels. *In* Current Topics in Membranes. I. Levitan, ed. Academic Press, pp. 187–208.

23. Barbera, N., M. A. A. Ayee, …, I. Levitan. 2018. Molecular dynamics simulations of Kir2.2 interactions with an ensemble of cholesterol molecules. *Biophys. J.* 115:1264–1280.

24. Corradi, V., B. I. Sejdiu, …, D. P. Tieleman. 2019. Emerging diversity in lipid–protein interactions. *Chem. Rev.* 119:5775–5848.

25. Hedger, G., H. Koldsø, …, M. S. P. Sansom. 2019. Cholesterol interaction sites on the transmembrane domain of the hedgehog signal transducer and class F G protein-coupled receptor smoothened. *Structure.* 27:549–559.e2.

26. Muller, M. P., T. Jiang, …, E. Tajkhorshid. 2019. Characterization of lipid–protein interactions and lipid-mediated modulation of membrane protein function through molecular simulation. *Chem. Rev.* 119:6086–6161.

27. Newport, T. D., M. S. P. Sansom, and P. J. Stansfeld. 2019. The MemProtMD database: a resource for membrane-embedded protein structures and their lipid interactions. *Nucleic Acids Res.* 47:D390–D397.

28. Rouviere, E., C. Arnarez, …, E. Lyman. 2017. Identification of two new cholesterol interaction sites on the A2A adenosine receptor. *Biophys. J.* 113:2415–2424.

29. Simonson, T. 2016. The physical basis of ligand binding. *In* In Silico Drug Discovery and Design. C. N. Cavasotto, ed. CRC Press, pp. 3–44.

30. Sutherland, J. J., R. K. Nandigam, …, M. Vieth. 2007. Lessons in molecular recognition. 2. Assessing and improving cross-docking accuracy. *J. Chem. Inf. Model.* 47:2293–2302.

31. Lomize, A. L., I. D. Pogozheva, …, H. I. Mosberg. 2006. Positioning of proteins in membranes: a computational approach. *Protein Sci.* 15:1318–1333.

32. Pettersen, E. F., T. D. Goddard, …, T. E. Ferrin. 2004. UCSF Chimera–a visualization system for exploratory research and analysis. *J. Comput. Chem.* 25:1605–1612.

33. Stevens, T. J., and W. Boucher. 2015. Python Programming for Biology: Bioinformatics and Beyond. Cambridge University Press, Cambridge, UK.

34. Tan, K. P., T. B. Nguyen, …, M. S. Madhusudhan. 2013. Depth: a web server to compute depth, cavity sizes, detect potential small-molecule ligand-binding cavities and predict the pKa of ionizable residues in proteins. *Nucleic Acids Res.* 41:W314–W321.

35. Guo, J., J. She, …, Y. Jiang. 2017. Structures of the calcium-activated, non-selective cation channel TRPM4. *Nature.* 552:205–209.

36. Zhang, Z., B. Tóth, …, L. Csanády. 2018. Structure of a TRPM2 channel in complex with Ca^{2+} explains unique gating regulation. *eLife.* 7:e36409.

37. Huang, Y., P. A. Winkler, …, J. Du. 2018. Architecture of the TRPM2 channel and its activation mechanism by ADP-ribose and calcium. *Nature.* 562:145–149.

38. Jorgensen, C., L. Darré, …, C. Domene. 2016. Lateral fenestrations in K(+)-channels explored using molecular dynamics simulations. *Mol. Pharm.* 13:2263–2273.

39. Wang, L., T. M. Fu, …, H. Wu. 2018. Structures and gating mechanism of human TRPM2. *Science.* 362:eaav4809.

40. Yin, Y., S. C. Le, …, S.-Y. Lee. 2019. Structural basis of cooling agent and lipid sensing by the cold-activated TRPM8 channel. *Science.* 363:eaav9334.

41. Hirschi, M., M. A. Herzik, Jr., …, S. Y. Lee. 2017. Cryo-electron microscopy structure of the lysosomal calcium-permeable channel TRPML3. *Nature.* 550:411–414.

42. Jansson, E. T., C. L. Trkulja, …, O. Orwar. 2013. Effect of cholesterol depletion on the pore dilation of TRPV1. *Mol. Pain.* 9:1–9.

43. Saha, S., A. Ghosh, …, C. Goswami. 2017. Preferential selection of Arginine at the lipid-water-interface of TRPV1 during vertebrate evolution correlates with its snorkeling behaviour and cholesterol interaction. *Sci. Rep.* 7:16808.

44. Gao, Y., E. Cao, …, Y. Cheng. 2016. TRPV1 structures in nanodiscs reveal mechanisms of ligand and lipid action. *Nature.* 534:347–351.

45. Zubcevic, L., M. A. Herzik, Jr., …, S. Y. Lee. 2018. Conformational ensemble of the human TRPV3 ion channel. *Nat. Commun.* 9:4773.

46. Zubcevic, L., S. Le, …, S. Y. Lee. 2018. Conformational plasticity in the selectivity filter of the TRPV2 ion channel. *Nat. Struct. Mol. Biol.* 25:405–415.

47. Svobodova, B., and K. Groschner. 2016. Mechanisms of lipid regulation and lipid gating in TRPC channels. *Cell Calcium.* 59:271–279.

48. Fan, C., W. Choi, …, W. Lü. 2018. Structure of the human lipid-gated cation channel TRPC3. *eLife.* 7:e36852.

49. Duan, J., J. Li, …, J. Zhang. 2018. Structure of the mouse TRPC4 ion channel. *Nat. Commun.* 9:3102.

50. Vinayagam, D., T. Mager, …, S. Raunser. 2018. Electron cryo-microscopy structure of the canonical TRPC4 ion channel. *eLife.* 7:e36615.

51. Fine, M., P. Schmiege, and X. Li. 2018. Structural basis for PtdInsP$_2$-mediated human TRPML1 regulation. *Nat. Commun.* 9:4192.

52. Jin, P., D. Bulkley, …, Y. Cheng. 2017. Electron cryo-microscopy structure of the mechanotransduction channel NOMPC. *Nature.* 547:118–122.

53. Wilkes, M., M. G. Madej, …, C. Ziegler. 2017. Molecular insights into lipid-assisted Ca^{2+} regulation of the TRP channel Polycystin-2. *Nat. Struct. Mol. Biol.* 24:123–130.

54. Simmonds, A. C., J. M. East, …, A. G. Lee. 1982. Annular and non-annular binding sites on the $(Ca^{2+} + Mg^{2+})$-ATPase. *Biochim. Biophys. Acta.* 693:398–406.

55. Zubcevic, L., M. A. Herzik, Jr., …, S. Y. Lee. 2016. Cryo-electron microscopy structure of the TRPV2 ion channel. *Nat. Struct. Mol. Biol.* 23:180–186.

56. Hughes, T. E. T., D. T. Lodowski, …, V. Y. Moiseenkova-Bell. 2018. Structural basis of TRPV5 channel inhibition by econazole revealed by cryo-EM. *Nat. Struct. Mol. Biol.* 25:53–60.

57. Dang, S., M. K. van Goor, …, J. van der Wijst. 2019. Structural insight into TRPV5 channel function and modulation. *Proc. Natl. Acad. Sci. USA.* 116:8869–8878.

58. McGoldrick, L. L., A. K. Singh, …, A. I. Sobolevsky. 2018. Opening of the human epithelial calcium channel TRPV6. *Nature.* 553:233–237.